

See discussions, stats, and author profiles for this publication at: <https://www.researchgate.net/publication/273783942>

Self-Assembly of a 9-Residue Amyloid-Forming Peptide Fragment of SARS Corona Virus E-protein: Mechanism of Self Aggregation and Amyloid-Inhibition of hIAPP.

ARTICLE *in* BIOCHEMISTRY · MARCH 2015

Impact Factor: 3.02 · DOI: 10.1021/acs.biochem.5b00061 · Source: PubMed

CITATIONS

2

READS

101

8 AUTHORS, INCLUDING:



Anirban Ghosh

Bose Institute

10 PUBLICATIONS 34 CITATIONS

[SEE PROFILE](#)



Jyotsna Bhat

Bose Institute

7 PUBLICATIONS 16 CITATIONS

[SEE PROFILE](#)



Ayyalusamy Ramamoorthy

University of Michigan

336 PUBLICATIONS 11,700 CITATIONS

[SEE PROFILE](#)



Anirban Bhunia

Bose Institute

67 PUBLICATIONS 912 CITATIONS

[SEE PROFILE](#)

¹ Self-Assembly of a Nine-Residue Amyloid-Forming Peptide Fragment of SARS Corona Virus E-Protein: Mechanism of Self Aggregation and Amyloid-Inhibition of hIAPP

⁴ Anirban Ghosh,^{†,§} Amit S. Pithadia,^{‡,§} Jyotsna Bhat,[†] Supriyo Bera,[†] Anupam Midya,[§] Carol A. Fierke,^{‡,||,⊥}
⁵ Ayyalusamy Ramamoorthy,^{‡,||} and Anirban Bhunia^{*†,‡,||}

⁶ [†]Department of Biophysics, Bose Institute, P-1/12 CIT Scheme VII (M), Kolkata 700 054, India

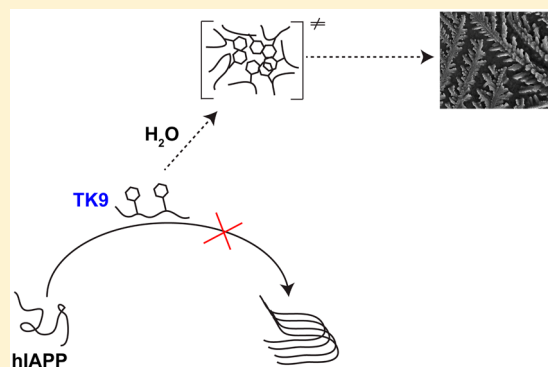
⁷ [‡]Department of Chemistry, ^{||}Department of Biophysics, and [⊥]Department of Biological Chemistry, University of Michigan, 930

8 North University Avenue, Ann Arbor, Michigan 48109-1055, United States

⁹ [§]School of Nanoscience and Technology, Indian Institute of Technology Kharagpur, Kharagpur 721302, India

10 Supporting Information

ABSTRACT: Molecular self-assembly, a phenomenon widely observed in nature, has been exploited through organic molecules, proteins, DNA, and peptides to study complex biological systems. These self-assembly systems may also be used in understanding the molecular and structural biology which can inspire the design and synthesis of increasingly complex biomaterials. Specifically, use of these building blocks to investigate protein folding and misfolding has been of particular value since it can provide tremendous insights into peptide aggregation related to a variety of protein misfolding diseases, or amyloid diseases (e.g., Alzheimer's disease, Parkinson's disease, type-II diabetes). Herein, the self-assembly of TK9, a nine-residue peptide of the extra membrane C-terminal tail of the SARS corona virus envelope, and its variants were characterized through biophysical, spectroscopic, and simulated studies, and it was confirmed that the structure of these peptides influences their aggregation propensity, hence, mimicking amyloid proteins. TK9, which forms a beta-sheet rich fibril, contains a key sequence motif that may be critical for beta-sheet formation, thus making it an interesting system to study amyloid fibrillation. TK9 aggregates were further examined through simulations to evaluate the possible intra- and interpeptide interactions at the molecular level. These self-assembly peptides can also serve as amyloid inhibitors through hydrophobic and electrophilic recognition interactions. Our results show that TK9 inhibits the fibrillation of hIAPP, a 37 amino acid peptide implicated in the pathology of type-II diabetes. Thus, biophysical and NMR experimental results have revealed a molecular level understanding of peptide folding events, as well as the inhibition of amyloid-protein aggregation are reported.



The formation of nanostructures through molecular self-assembly has been demonstrated to be a ubiquitous process in nature as seen by organic molecules (polymers), proteins, peptides, and DNA. These nanostructures have been characterized by their highly ordered aggregate formation through noncovalent interactions (e.g., electrostatic, hydrogen bonds, van der Waals, and aromatic π -stacking and cation- π). The emerging field of nanotechnology has exploited self-assembly systems due to the key advantage that their physical, chemical, optoelectronic, magnetic, and mechanical properties are tunable via control of their size and shape.¹ Interestingly, all the aforementioned noncovalent forces are quite weak in nature, individually, but cumulatively they support the self-organization of simple units into complicated and controlled structures.² Despite tremendous research efforts, the relative involvement of these forces in self-assembly processes is yet to be more clearly understood. Recently, substantial attention has been intended for the rational design and structural analysis of

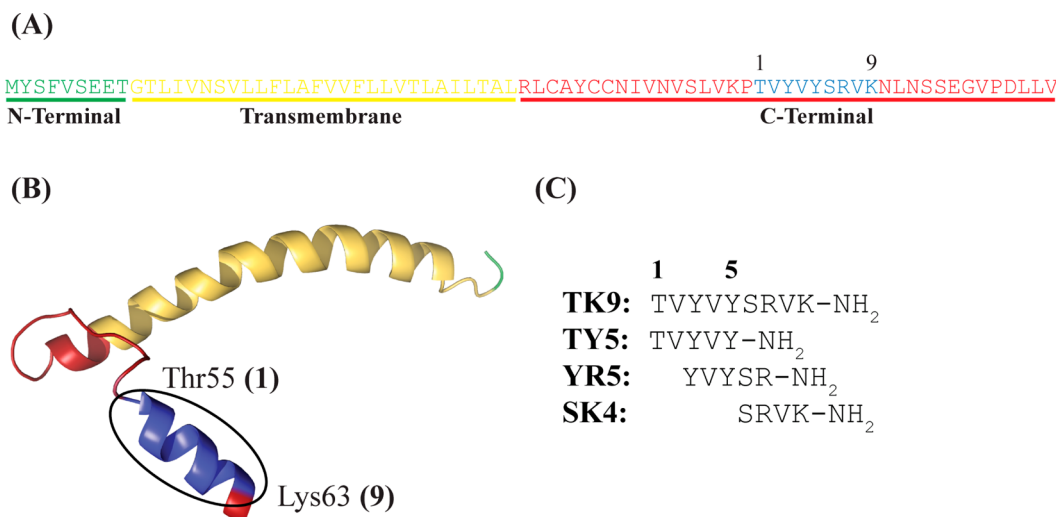
peptide-based self-assembly due to their widespread diversity in chemical, structural, and functional aspects.^{1,3} Furthermore, the complex nature of biomolecules limits the comprehensive understanding of the factors controlling the self-assembling properties. To examine this in more detail, short peptides or peptide fragments can be constructed relatively quickly and may serve as the competent building blocks for self-assembled systems, thus avoiding the complexities of forming and studying large protein structures.

Self-assembled peptide systems have also been utilized in studying protein-folding events in order to provide insight into the thermodynamic properties of protein folding and misfolding. These investigations have also helped gain information about specific structural motifs adopted by specific

Received: January 22, 2015

Revised: March 16, 2015

Scheme 1. (A) SARS CoV-E Sequence with the TK9 Region Shown in Blue, (B) The Three-Dimensional Solution Structure of SARS CoV-E Protein in Sodium Dodecyl Sulfate (SDS) Micelle,^a and (C) The Primary Amino Acid Sequence of TK9 or Its Shorter Fragments



^a2MM4.pdb. The C-terminal tail, Thr55–Lys63 adopted alpha helical conformation in micelle, marked by circle, used in this study.

64 amino acid sequences and combinations which may be
65 responsible for protein misfolding and amyloid formation.
66 Therefore, studying the self-assembly of peptides has been
67 utilized as an important tool for analyzing the local structure
68 (e.g., secondary structure) of peptide fragments in the context
69 of the global protein structure.⁴ These peptide nanostructures
70 are generally formed from beta (β)-sheet motifs, although a few
71 helical-based assemblies have also been reported.⁵⁻⁸ On the
72 basis of various structural, chemical, and physical properties,
73 they are classified according to the following categories: (a)
74 lipid-like peptides, (b) surfactant peptides, (c) amphiphilic
75 peptides, (d) aromatic dipeptide motifs, (e) cyclodextrin-based
76 polyionic amino acids from known self-assembled proteins, (e)
77 cyclic peptides, and (f) arbitrarily chosen peptide sequence
78 based on amino acid properties.⁹ The unique supramolecular
79 assemblies can be readily tuned by modifying structural
80 properties such as changing the amino acid sequence or
81 conjugating chemical groups or by varying experimental
82 parameters such as pH or solvent. Peptide nanostructures
83 have also been utilized in vast miscellaneous fields, from
84 antibacterial agents to molecular electronics, with a great
85 achievement and therefore have become of great interest to
86 study.^{10,11}

87 Importantly, investigating self-assembly systems at the
 88 molecular level have been of particular value in studying the
 89 complex phenomena behind the aggregation of amyloid
 90 proteins and aggregation of other proteins related to fatal
 91 protein conformational disorders.¹² It has been found that
 92 amyloid-related diseases (e.g., Alzheimer's disease (AD), prion
 93 diseases, Type II diabetes, Parkinson's disease, and Hunting-
 94 ton's disease) are connected by the aggregation of relatively
 95 unstructured monomers into a β -sheet-rich fibrillar aggre-
 96 gates.^{13,14} In spite of the diversity in sequence homology, the
 97 fibrillar networks have similar morphologies; however, the
 98 precise biochemical/biophysical pathways and mechanism of
 99 protein fibrillation still remain elusive. Self-assembled short
 100 peptides have the potential to serve as model systems to
 101 studying amyloid aggregation by simplifying the study of
 102 amyloidosis as seen in a study by Lynn and co-workers.¹⁵ This

can help probe specific protein–protein interactions between 103 the small peptide assemblies and translate this information to 104 elucidating the aggregation properties of the native peptide/ 105 protein. Furthermore, small peptide fragments from amyloid 106 proteins (KLVFF in amyloid- β and NFGAIL in hIAPP) have 107 been demonstrated to have inhibitory properties, thus 108 modifying or in some cases halting the aggregation pathway. 109 Therefore, studying self-assembled peptide fragments may also 110 help potentially uncover possible motifs that may be utilized for 111 amyloid inhibition and eventually therapeutic applications. 112

In the present study, we have investigated and analyzed the self-assembly of a nine-residue peptide (hereafter denoted as TK9) and its derivatives taken from the sequence of the carboxyl terminal (55–63) of SARS corona virus envelope protein (Scheme 1).¹⁶ Generally, corona viruses are enveloped and this enveloped (E) region may be the main culprit in causing virulence related to various respiratory diseases such as common colds, bronchiolitis, and acute respiratory distress syndrome in humans and others.¹⁷ The E regions are peptide fragments consisting of 76–108 amino acids and composed of a flexible region at both N- and C-terminals and α -helical transmembrane (TM) region.¹⁸ This region has been shown to adopt a mainly helical structure in the presence of SDS micelles, suggesting that a membrane surface may influence its secondary structure.¹⁸ Upon mutation of the $^{56}\text{VYVY}^{59}$ region of the C-terminal tail in the SARS corona virus, the secondary structure has changed to a more discrete β -structure.¹⁸

To gain further insight about whether the short peptide, 130 TK9, and its variants have a self-assembling tendency, we 131 carried out detailed biophysical and high resolution analyses of 132 TK9. These data demonstrated that TK9 self-assembles and 133 forms a β -sheet secondary structure in solution. To support our 134 experimental findings and also to extract the atomic level 135 interactions acting as a driving force for this self-assembly 136 process, we performed molecular dynamics (MD) simulations. 137 Furthermore, we also studied the ability of TK9 to inhibit the 138 aggregation of a 37-residue human islet amyloid polypeptide 139 protein (hIAPP) in order to obtain possible structural motifs 140 that may be beneficial for the mitigation of hIAPP aggregation. 141

142 Previous studies have shown that unstructured hIAPP
143 monomers aggregate to form toxic intermediates and amyloid
144 fibers that composed of β -sheet peptide structures that are
145 implicated in type II diabetes. Therefore, there is considerable
146 current interest in developing compounds to inhibit hIAPP
147 aggregation and islet cell toxicity. In this context, the amyloid-
148 inhibiting ability of TK9 could be useful and aid in the
149 development of potent amyloid inhibitors.

150 ■ MATERIALS AND METHODS

151 **Materials and Preparation of Stock Solutions.** The
152 parent peptide, TK9, and its shorter fragments (Scheme 1)
153 were synthesized on a solid phase peptide synthesizer (Aapptec
154 Endeavor 90) using Fmoc protected amino acids and Rink
155 Amide MBHA resin (substitution 0.69 mmol/g; Novabiochem,
156 San Diego, California) by following a solid phase peptide
157 synthesis protocol described elsewhere.^{19,20} The C-termini of
158 the peptides are amidated. All the crude peptides were further
159 purified by reverse phase HPLC (SHIMADZU, Japan) using a
160 Phenomenex C18 column (dimension 250 × 10 mm, pore size
161 100 Å, 5- μ m particle size) by linear gradient elution technique
162 using Water and Methanol as solvent both containing 0.1%
163 TFA as the ion pairing agent. The purity and molecular weight
164 of the eluted peptides were confirmed by MALDI-TOF
165 (Bruker, Germany). 4,4-Dimethyl-4-silapentane-1-sulfonic acid
166 (DSS) and deuterium oxide (D_2O) were purchased from
167 Cambridge Isotope Laboratories, Inc. (Tewksbury, MA).
168 Thioflavin T dye was purchased from Sigma-Aldrich (St.
169 Louis, MO). Throughout the experiment HPLC grade water
170 was used for sample preparation. hIAPP was purchased from
171 Genscript (Piscataway, NJ). hIAPP was prepared by dissolving
172 the peptide in hexafluoroisopropanol (Sigma-Aldrich) followed
173 by lyophilization. Peptide stock was dissolved in 100 μ M HCl
174 (pH 4), sonicated for 1 min, diluted into the appropriate buffer
175 system, and kept on ice until use.

176 **Circular Dichroism.** All circular dichroism experiments
177 were performed on Jasco J-815 spectrometer (Jasco Interna-
178 tional Co., Ltd. Tokyo, Japan) furnished with a Peltier cell
179 holder and temperature controller CDF-426L at 25 °C. The
180 peptide concentrations were 25 μ M for all CD measurements.
181 The samples were scanned between 190 to 260 nm wavelength
182 at a scanning speed of 100 nm min⁻¹. The data interval was 1
183 nm and path length 2.0 mm. All data-points are the result of an
184 average of four repetitive scans. All experiments were
185 performed in 10 mM phosphate buffer of pH 7.0. Each
186 spectrum was baseline corrected with reference to buffer. The
187 data obtained in mill degrees were converted to molar ellipticity
188 (ME) (deg·cm²·dmol⁻¹) and plotted against wavelength (nm).

189 **Fluorescence Assays.** Tyrosine fluorescence experiments
190 were performed using Hitachi F-7000 FL spectrometer with a
191 0.1 cm path length quartz cuvette at 25 °C. Intrinsic tyrosine
192 fluorescence property was used to monitor the self-assembly
193 property for tyrosine containing peptides TK9, TYS, YRS using
194 an excitation wavelength of 274 nm and emission in a range of
195 290–370 nm.²¹ The excitation and emission slit both were 5
196 nm. The peptide concentrations were 25 μ M throughout the
197 experiment. Thioflavin-T (ThT) experiments were performed
198 on a BioTek multiplate reader using an excitation wavelength of
199 440 nm and emission wavelength of 485 nm. Samples were
200 prepared by adding hIAPP (10 μ M) to a buffer solution (10
201 mM phosphate, 150 mM NaCl, pH 7.4) containing ThT (20
202 μ M) and varying concentrations of TK9 monomer (0.5–2

equiv). TK9 aggregates for the ThT assay were prepared by
203 incubation at 37 °C for 7 days.

204 **Dynamic Light Scattering.** DLS experiments were
205 performed using Malvern Zetasizer Nano S (Malvern Instru-
206 ments, UK) equipped with a 4 mW He-Ne gas laser (beam
207 wavelength = 632.8 nm) and 173° back scattering measurement
208 facility. All samples were filtered using 0.25- μ m filter paper
209 (Whatman Inc., NJ) and degassed before use and measured at
210 298 K using a low volume disposable sizing cuvette. The
211 peptide concentration was kept at 10 μ M in phosphate buffer
212 (pH 7.0) during the duration of the experiment.

213 **Nuclear Magnetic Resonance.** The synthetic peptide,
214 TK9, and its analogues were dissolved in milli-Q water (pH
215 7.0). All NMR spectra were recorded at 298 K using Bruker
216 Avance III 500 MHz NMR spectrometer, equipped with a 5
217 mm SMART probe. Two-dimensional total correlation spec-
218 troscopy (TOCSY) and rotating frame nuclear Overhauser
219 effect spectroscopy (ROESY) spectra of TK9 were acquired in
220 water containing 10% D_2O and 2,2-dimethyl-2-silapentane 5-
221 sulfonate sodium salt (DSS) as an internal standard (0.0 ppm
222 for methyl protons). The peptide concentration was kept at 1
223 mM for the sequential assignment and relaxation studies,
224 respectively. TOCSY mixing time was set to 80 ms using the
225 MLEV-17 spin-lock sequence to ensure coherence transfer via
226 scalar couplings, whereas a 150 ms spin-lock mixing time was
227 used for ROESY experiments. The TOCSY and ROESY
228 experiments were performed with 456 t1 increments and 2048
229 t2 data points. The residual water signal was suppressed by
230 excitation sculpting techniques. The spectral widths were set to
231 10 ppm in both dimensions with a saturation delay of 1.5 s.
232 Data acquisition and data processing were carried out using
233 Topspin v3.1 software (Bruker Biospin, Switzerland).

234 The two-dimensional NMR data were assigned and analyzed
235 using SPARKY²² program. The cross peak intensities measured
236 from ROESY spectra were qualitatively classified as strong,
237 medium, and weak, which were then converted to upper bound
238 distance limits of 3.0, 4.0, and 5.5 Å, respectively. The lower
239 bound distance was constrained to 2.0 Å to avoid van der Waals
240 repulsion. The backbone dihedral angle (phi, ϕ) was varied
241 from -30° to -120° to restrict the conformational space for all
242 residues. Finally, Cyana 2.1 software was used for structure
243 calculation with the help of distance and dihedral angle
244 restraints.²³ Several rounds of refinement were performed
245 based on the NOE violations, and the distance constraints were
246 accustomed accordingly. A total of 100 structures were
247 calculated, and 20 conformers with the lowest energy values
248 were selected to present the NMR ensemble and starting
249 structure for coarse grain molecular dynamics simulation.

250 A series of one-dimensional proton NMR spectra for TK9
251 and its analogues were recorded at different time intervals to
252 determine their aggregation tendency. The spectra were
253 acquired with water suppression with a spectral width of 12
254 ppm, 128 transients, a relaxation delay of 1.5 s. The spectra
255 were processed and plotted with TopSpin software (Bruker,
256 Switzerland) using a line broadening of 1.0 Hz.

257 Saturation transfer difference (STD) NMR experiments for a
258 sample containing TK9 (0.5 mM) and hIAPP monomers (10
259 μ M) were carried at 25 °C for 12 h consecutively with an
260 interval of 15 min using a Bruker 600 MHz NMR spectrometer
261 equipped with a cryo probe. The peptide, hIAPP or its fibril was
262 irradiated at -1 (on-resonance) and at 40 ppm (off-resonance)
263 for a duration of 2 and 128 scans were coadded to get the
264 spectrum. The selective irradiation was achieved by a train of
265

266 Gaussian pulses with 1% truncation for a duration of 49 ms
267 with an interval of 1 ms at 50 dB.

268 **Relaxation Studies.** To gain access the atomic level
269 dynamics present one-dimensional spin–spin (T_1) and spin–
270 lattice (T_2) relaxation experiments for TK9 were performed
271 using 500 MHz Bruker Avance III NMR spectrometer. T_1
272 experiments were performed using the same protocol that we
273 published earlier with different inversion recovery delays
274 starting from 50 ms to 5 s.²⁴ Similarly, T_2 measurements
275 were carried out using the CPMG sequence for a set of delays:
276 2, 6, 32, 100, 200, 400, 800, 2000, 3000, and 4000 ms.²⁵

277 **Scanning Electron Microscopy (SEM).** The incubated
278 peptide solutions were deposited on a glass slide (1 cm²) and
279 dried oven night in air. The slide was then coated with gold for
280 120 s at 10 kV voltage and 10 mA current. The samples were
281 viewed on a ZEISS EVO-MA 10 scanning electron microscope
282 equipped with a tungsten filament gun operating at 10 kV.

283 **Transmission Electron Microscopy (TEM).** The 500 μM
284 peptide stock solutions were incubated at room temperature for
285 up to 15 days and 10 μL aliquots of the solution were placed on
286 300 mesh Formvar/carbon coated copper TEM grids (Ted
287 Pella, Redding, CA 96049, USA). It was allowed to adsorb on
288 TEM grid for about 3–4 min, and excess volume was removed
289 with filter paper. The grid was negatively stained with 5% (v/v)
290 freshly prepared uranyl acetate in water. After 5 min excess dye
291 was removed, and the grids were viewed on a JEOL JEM 2100
292 HR TEM microscope operating at 80 kV. A set of TEM
293 samples for TK9 were also viewed on a Philips Model CM-100
294 transmission electron microscope (80 kV, 25000 \times magnifica-
295 tion). Digital images were acquired using Gatan Digital
296 Micrograph 2.3.0 image Capture Software.

297 **Coarse-Grained Molecular Dynamics Simulations.**

298 Coarse-grained (CG) molecular dynamics (MD) simulation
299 of TK9 was performed using Martini model.^{26,27} Using this
300 model, TK9 is mimicked by 24 beads in a single chain, as
301 shown in Figure S1, Supporting Information. Simulation
302 systems were built with 20 chains of beaded TK9 placed
303 randomly in a box of size 12 nm. Energy minimization was
304 initially conducted on peptide in a vacuum using the steepest
305 descent method with a maximum step size of 0.01 nm and a
306 force tolerance of 10 kJ mol⁻¹ nm⁻¹. Solvation of the system
307 was carried out with 59652 CG water molecules (each CG
308 water molecule corresponds to 4 all atom water molecules).
309 The solvated system was further minimized using the same
310 parameters as that of energy minimization in a vacuum. Then
311 MD simulation was performed using NPT. The velocities were
312 assigned according to the Maxwell–Boltzmann distribution at
313 320 K. Temperature was kept at 310 K by the Berendsen
314 method with a time constant of 0.3 ps, and the pressure was
315 maintained at 1 bar with a time constant of 3 ps and a
316 compressibility of 3×10^{-5} bar⁻¹. The periodic boundary
317 conditions (PBC) were applied. The nonbonded Lennard–
318 Jones (LJ) and electrostatic interactions were calculated using a
319 cut off of 1.2 nm. Furthermore, the standard shift function in
320 GROMACS was used to reduce undesired noise.²⁸ Specifically,
321 the LJ potential and electrostatic potentials were shifted to zero
322 from 0.9 and 0.0 nm, respectively, to the cut off distance (1.2
323 nm). A time step of 30 fs was used and the trajectory was saved
324 every 150 ps for analysis. The simulation duration was 1 μs .
325 Structural changes in the assembly during the simulation run
326 are captured at different time steps as shown in Figure S2,
327 Supporting Information.

328 **Reverse Construction of All Atom System.** Reconstruc-
329 tion of all atom (AA) system from CG was carried out to regain
330 the atomic details. At first, AA particles were placed near to the
331 corresponding CG beads and coupled to CG beads by
332 harmonic restraints. This restrained the system further and
333 then was processed by simulated annealing (SA); the final
334 relaxed atomic model was obtained by the gradual removal of
335 the restraints.²⁹

336 There construction simulations started from the snapshot at
337 999 ns time step of the CG simulations as illustrated in Figure
338 S3, Supporting Information. The atomistic simulations were
339 carried out with a 2 fs integration time step, and the
340 temperature was controlled by coupling to a Nosé–Hoover
341 thermostat with a time constant of 0.1 ps.³⁰ Because of the
342 random initial placement of the atomistic particles, no
343 constraints were applied in the reconstruction simulations,
344 except for SPC water.

345 For the simulations of the TK9, the 53 a6 parameter set of
346 the GROMOS united atom force field was used.³¹ The system
347 was simulated within periodic boundary conditions. Non-
348 bonded interactions were calculated using a triple-range cut off
349 scheme: interactions within 0.9 nm were calculated at every
350 time step from a pair list, which was updated every 20 fs. At
351 these time steps, interactions between 0.9 and 1.5 nm were also
352 calculated and kept constant between updates. A reaction-field
353 contribution was added to the electrostatic interactions beyond
354 this long-range cut off, with $\epsilon_r = 62$. In the simulations of bulk
355 SPC water, a win range cut off scheme was used, with a single
356 cut off at 0.9 nm and a pair list updated every 20 fs. Here, a
357 long-range dispersion correction was applied in addition to the
358 reaction field. Other simulation parameters are as given in
359 Table S1, Supporting Information.

360 ■ RESULTS

361 **Design Considerations for TK9 and Its Variants.** The
362 SARS-CoV envelope region (Cov E) (Scheme 1a) contains a
363 relatively hydrophobic C-terminal region (Scheme 1B),
364 composed of an α helix (α -helix) at the trans-membrane
365 followed by a β -structured region,⁵⁵ TVYVYSRVK⁶³, or TK9,
366 which has been considered an essential sequence content for its
367 function. This region has been predicted to be responsible for
368 directing the protein to the Golgi region.^{18,32,33} It should be
369 mentioned that this type of motif remains conserved in other
370 corona viruses and is abundantly expressed in infected cells and
371 may also be critically involved in viral protein assembly.^{34,35}
372 Fourier transform infrared (FT-IR) spectroscopy investigations
373 have also shown that this portion of the protein can intrinsically
374 adopt both a random coil and β -sheet conformation in the
375 absence of a membrane environment.³² The folding domain (β -
376 structured region), which contains the sequence of TVYVY-
377 SRVK and its fragments (Scheme 1B), contains residues and
378 sequences similar to those of amyloid proteins. This has led to
379 the hypothesis that TK9 may have similar properties to the
380 folding domains of amyloid proteins (e.g., amyloid- β), where
381 certain residue regions have limited water solubility and adopt a
382 β -sheet structure and may aggregate to form amyloid-like
383 fibrillar species. This observation has made TK9 and its
384 derivatives insightful nanostructure systems to study protein
385 assembly and mechanism of folding.³⁶ Specifically, residues
386 I46–V62 contain branched and bulky side chains which may
387 favor the formation of β -sheet structures.³⁷ The first five
388 residues of TK9, TY5 (TVYVY) (Scheme 1C) also contain a
389 peptide motif demonstrated to form amyloid-like fibrils;
390

therefore, this short peptide fragment and its derivatives, namely, TY5, YRS, and SK4 (Scheme 1C), were chosen as model systems to give possible insights into amyloid folding events. These sequence motifs containing branched, hydrophobic residues as well as residues, which can form H-bonds, have been shown to have a higher aggregation propensity as seen with a Leu-Enkephalin mutant and VEALYL.^{38–41}

TK9 and TY5 Are More Prone to Aggregation with Increased Incubation Time. Dynamic light scattering (DLS) is an analytical method used to establish the size distribution of an ensemble of particles from Brownian motion property in solution.⁴² Here, we employed DLS to access the size distribution of the supramolecular structures formed during different incubation periods. It is seen that freshly prepared TK9 or its analogues, TY5, YRS, and SK4 (Scheme 1C) show a narrow size distribution pattern with a hydrodynamic diameter of ~27 nm (Figure 1A and Figure S4, Supporting Information). The narrow distribution confirms that the peptides are monomer in freshly dissolved solution at early time points. However, with increasing the incubation time period for TK9, TY5, and YRS, the size distribution profile became wider, which accounts for the presence of polymeric subunits in solution (Figure S4). After 15 days of incubation, clear distinctions in

the hydrodynamic diameters were observed for the peptides. TK9 and TY5 showed the highest change in hydrodynamic diameter, whereas YRS showed a moderate change in size distribution only after 25 days of incubation (Figure S4). On the other hand, SK4 showed a negligible amount of change in hydrodynamic diameter within a period of 25 days of incubation, which suggests its lower aggregating propensity. This trend pointed out that aromatic amino acids (Tyr) of these peptides may contribute significantly to the shape and size of their nanostructure assemblies and that polar amino acids may not directly influence their size. Overall, our DLS results proved a similar aggregation behavior of the parent peptide TK9 and its N-terminal fragments TY5 and YRS can be seen after 25 days of incubation.

Furthermore, circular dichroism (CD) spectroscopy was used to monitor the secondary structure of the peptide fragments at different incubation time (Figure 1B–E). Freshly prepared TK9 and its truncated shorter fragments showed a strong negative maximum at ~195 nm, characteristic of random coil conformation of the peptides or proteins (Figure 1B–E). Interestingly, after 15 days of incubation, samples containing TK9 and TY5 showed a distinct β -sheet type CD spectral signature consisting of positive maximum at 200 nm and a negative maximum at 215 nm due to $n-\pi^*$ and $\pi-\pi^*$ transition (Figure 1B,C). In contrary, the CD spectrum of YRS showed two peaks, one at ~198 nm and another broad peak at ~215 nm (Figure 1D). Similarly, SK4 showed a large broadening of peaks (Figure 1E). This result clearly signifies that both YRS and SK4 are highly dynamic in nature, and there may be conformational exchange between random coils to β -sheet in a dynamic state (Figure 1D,E). Overall the CD data identified that TK9 and TY5 undergo structural reorganization from random coil to β -sheet over time, while the other fragments are not prone to this similar conformational change.

Morphology of TK9 and Its Variants. To understand further about the morphological change of the nanostructures of the peptide self-assembly, various electron microscopic techniques such as transmission electron microscopy (TEM) and scanning electron microscopy (SEM) were employed. TEM data revealed that freshly prepared TK9 did not show any measurable structure (data not shown), which is in very good agreement with the CD data (Figure 1B). However, TEM analysis of the sample containing TK9 alone with 10 days of incubation displayed a dense fibrillar network which has slight amorphous and unbranched characteristics (Figure 2A and inset, respectively), suggesting that the peptide region is able to form β -sheet morphology, which could be in good agreement with the TEM images of β -sheet forming amyloid fibrils originated from either A β or hIAPP.⁴³ The effect of fibrillation was pronounced for both TK9 and TY5 which contain beta branched amino acids such as Thr1-Val2-Tyr3-Val4-Tyr5 residues. In addition, these residues are prone to form a plane of β -sheet structures (Figure 2B). The structure of TK9 emphasized that the rate of nucleation for the β -sheet formation could be slower due to the presence of two positive charge residues, Arg7 and Lys9 at the C-terminal of the peptide sequence, but our DLS data suggest that they fibrilize with similar kinetics. In contrast, YRS and SK4 did not show any defined nanostructure by TEM (data not shown), which could be attributed to the sole presence of charged residues at the C-terminal of TK9 sequence which did not allow the peptides to self-assemble.

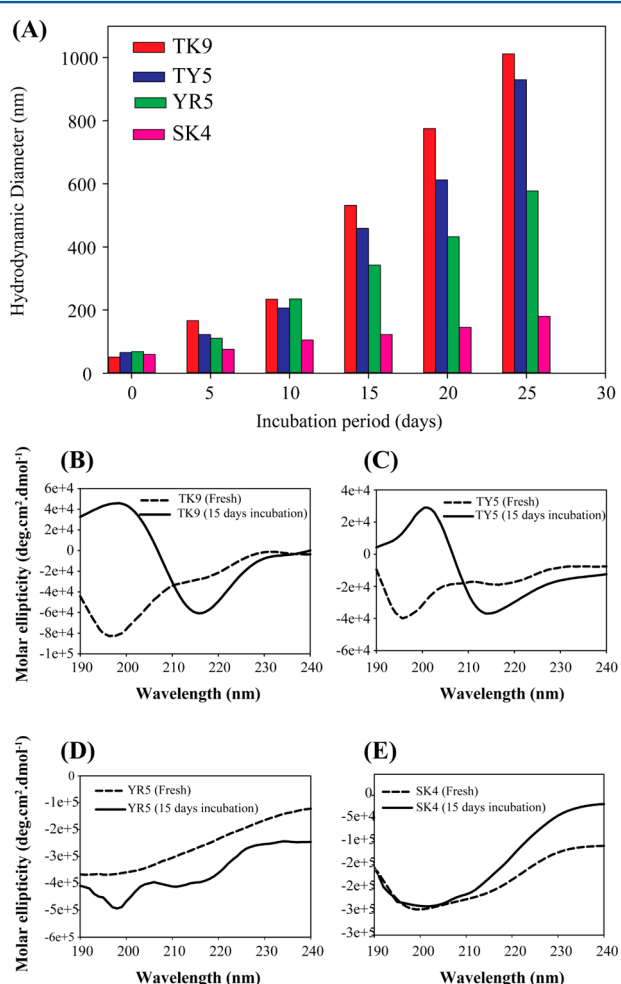


Figure 1. (A) Dynamic light scattering (DLS) plot for TK9 (red), TY5 (blue), YRS (green), and SK4 (pink); the intensity vs size distribution bar diagram are plotted at different time intervals. (B–E) Circular dichroism (CD) plots of secondary structure of TK9 and its fragments measured after freshly preparation and incubation with 15 days.

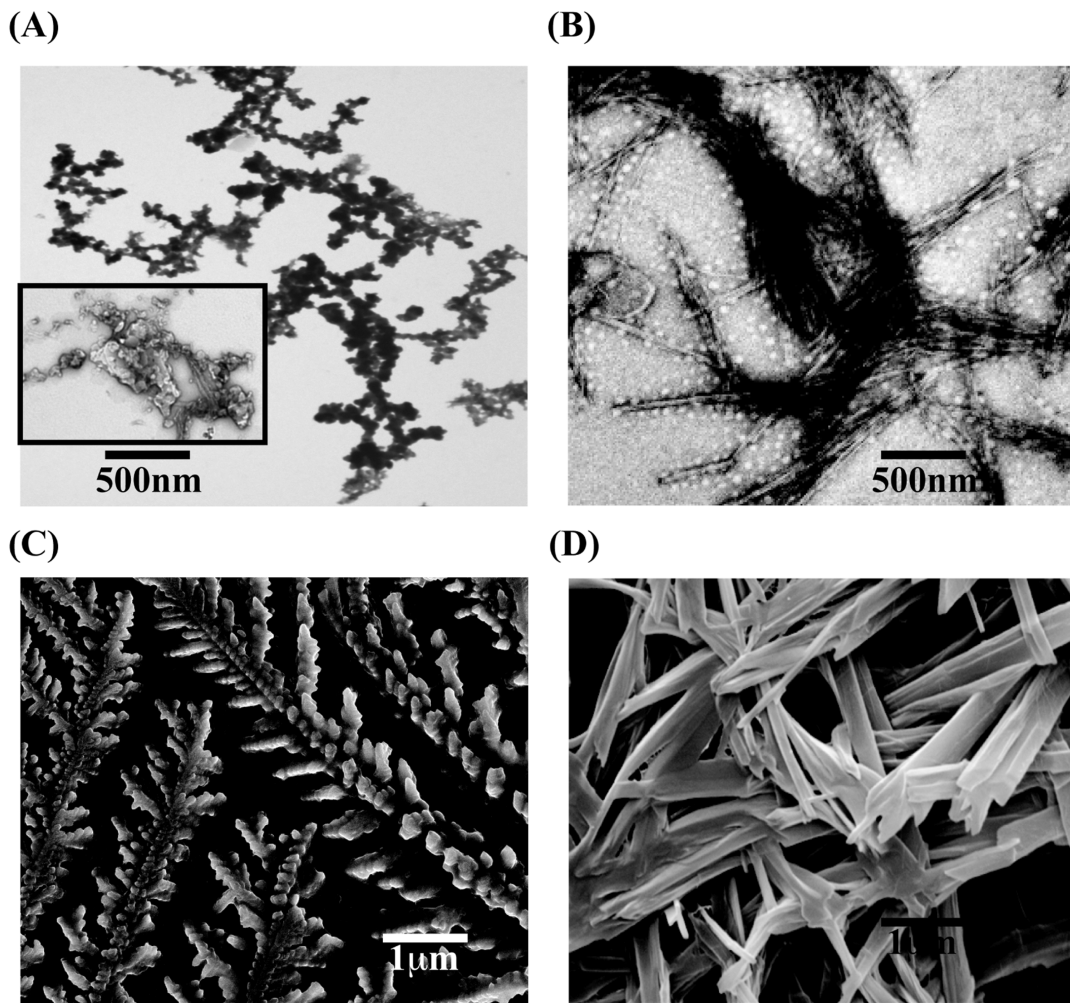


Figure 2. Transmission and scanning electron micrographs showing fibrillar nanostructure morphology for TK9 (A and C) and TY5 (B and D), respectively.

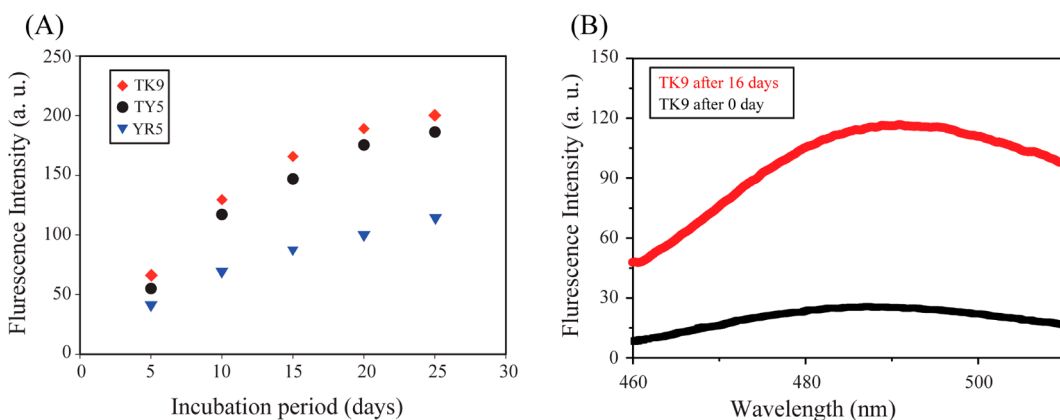


Figure 3. (A) Tyrosine fluorescence of TK9 (red), TY5 (black), and YRS (blue) monitoring increase in Tyr fluorescence signal as peptide aggregates. (B) Thioflavin T (ThT) fluorescence assay measuring β-sheet-rich fibril formation of freshly dissolved TK9 (black) and after 16 days of TK9 incubation (red).

Subsequently, SEM experiments were performed to understand the self-assembly propensity of TK9 and its analogues after incubation at 37 °C for several days (Figure 2C,D). TK9 exhibited well-defined, branched, long rod-like fibers (Figure 2C) after 25 days. The truncated analogue TY5 showed a dense nanotubular architecture (Figure 2D). These results indicate that both TK9 and TY5 form fibrils in solution. In contrary, the

central region of the peptide sequence YRS showed an amorphous-like architecture rather than uniformly well-defined fibers and tubes (Figure S5, Supporting Information). The C-terminal truncated peptide SK4 consisting of the charged residues (Ser6, Arg7, and Lys9) did not allow the peptide to adopt any particular structure (Figure S5). Taken together,

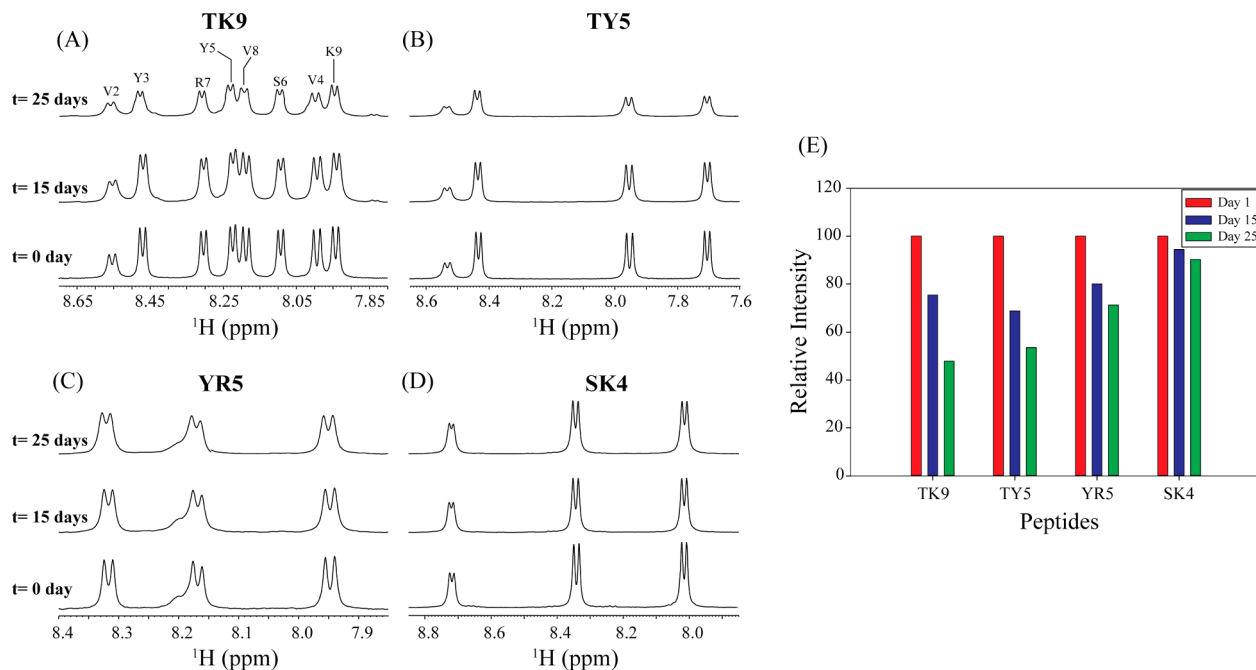


Figure 4. (A) Amide proton chemical shift regions of ^1H NMR spectra of TK9 (A), TY5 (B), YR5 (C), and SK4 (D); (E) average decrease in peak intensity for each peptide. Spectra obtained after 0, 15, and 25 days incubation period are overlaid.

488 TK9 and TY5 self-assembled to adopt a well-defined
489 nanostructure confirmed by both TEM and SEM.

490 Fluorescence Measurements to Monitor Peptide

491 **Aggregation.** The intrinsic fluorescence property of tyrosine
492 (Tyr) for TK9, TY5, and YR5 was used as a probe to determine
493 structural perturbation of the peptides upon incubation and the
494 putative role of the interactions involved. It is noteworthy to
495 mention that there are two Tyr residues in each of the peptide.
496 The intensity for emission maxima of Tyr was increased
497 gradually with increasing the incubation time period for TK9 as
498 well as TY5 and YR5 (Figure 3A). This enhancement was
499 attributed to the change in the local environment of the
500 fluorophore from a hydrophilic to a more hydrophobic
501 environment. Initially, the Tyr residues were randomly oriented
502 in solution where solvent molecule could easily quench their
503 fluorescence intensity. However, the fluorescence emission
504 maxima increased almost 4 times for TK9 and TY5 from 5 days
505 of incubation time to 25 days of incubation time (Figure 3A).
506 In contrast, the emission maxima of YR5 increased much less
507 compared to that of TK9 (Figure 3A). Conversely, the
508 incremental increase in fluorescence intensity of emission
509 maxima for YR5 was negligible and reached a plateau after 25
510 days of incubation (Figure 3A), suggesting YR5 may not form
511 an ordered aggregate in solution.

512 Furthermore, thioflavin T (ThT) assays was performed to
513 measure the higher order aggregation of TK9 over time. It is
514 noteworthy to mention that ThT is small molecule and
515 specifically binds to the β -sheet rich amyloid fibrils.⁴⁴ Figure 3B
516 shows the fluorescence intensity of ThT, binding to peptide,
517 TK9. The freshly dissolved TK9 incubated with ThT
518 demonstrated very low fluorescence intensity. However, as
519 TK9 was allowed to self-assemble for 16 days, a greater extent
520 of fluorescence intensity of ThT at approximately 490 nm was
521 displayed, indicative of the presence of a β -sheet rich species.
522 This result further confirms that the aggregation propensity of
523 TK9 in solution increases over time. Collectively, these results
524 suggest that the noncovalent $\pi-\pi$ stacking interaction between

525 the Tyr residues in the supramolecular structures of the
526 aggregated states create a hydrophobic environment (β -sheet
527 structure) where the entrance of water molecule is restricted
528 and hence enhances the fluorescence emission maxima and
529 interacts with the ThT dye.

530 ^1H NMR confirms the aggregation propensity of TK9. NMR
531 spectrum of TK9, or its analogues, exhibited well-resolved
532 narrow amide proton peaks indicating that the peptides are
533 highly dynamic in aqueous solution (Figure 4). A 2D TOCSY,
534 in conjunction with ROESY, spectrum was used to assign the
535 peaks (Figure S6). The ROESY spectrum of TK9 contained
536 intraresidue αN (i, i) as well as sequential, αN (i, i+1) ROEs
537 between backbone and side chain resonances (Figure S6A), and
538 no medium range αN (i to i+2/i+3/i+4) or long-range αN (i to
539 $\geq i+5$) cross peaks were observed, indicating that the peptide
540 does not adopt any folded conformation (Figures S6 and S7).
541 In addition, $\Delta H\alpha$ values of the residues did not show any
542 pattern of secondary structure (data not shown). A total of 47
543 ROEs (Table S2) were used to calculate the random coil
544 structure of TK9 (Figure S7), which is also confirmed by the
545 CD data (Figure 1).

546 To determine the extent of aggregation as a function of time,
547 we collected a series of 1D ^1H NMR spectra of all the peptides
548 in different time intervals of incubation. Figure 4 shows the
549 amide proton chemical shift regions for TK9 and its analogues
550 at the same time intervals. While freshly prepared peptides
551 exhibited well-dispersed narrow peaks from amide protons, line
552 broadening was observed with time of incubation (Figure 4A–
553 D). TK9 and TY5 showed the highest amount of line
554 broadening with respect to time, whereas SK4 showed the
555 least line broadening (Figure 4E). The observed line broad-
556 ening in NMR spectra could be due to the formation of high
557 molecular weight peptide aggregation. This effect was further
558 confirmed by proton relaxation studies.

559 ^1H NMR relaxation studies are used extensively as a sensitive
560 probe to investigate the weak interactions (dissociation
561 constant, $K_d \approx \mu\text{M}$ to mM range) in peptide oligomerization.⁴⁵

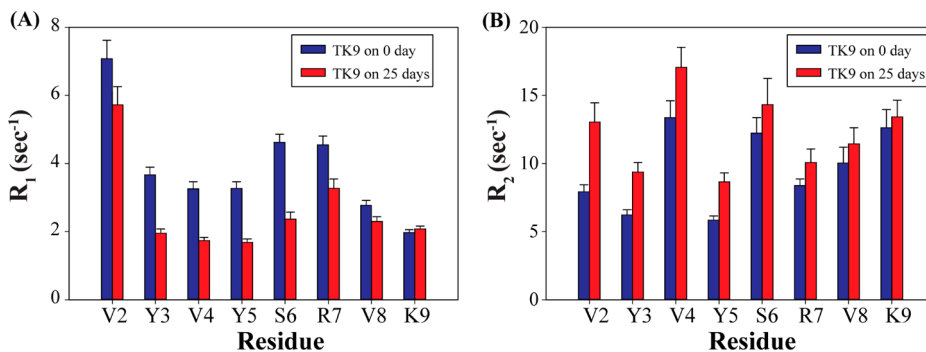


Figure 5. Residue-wise relaxation profile for freshly prepared TK9 (blue) and 25 days incubated TK9 (red). (A) Longitudinal relaxation rate (R_1) and (B) transverse relaxation rate (R_2) are plotted for each residue of TK9.

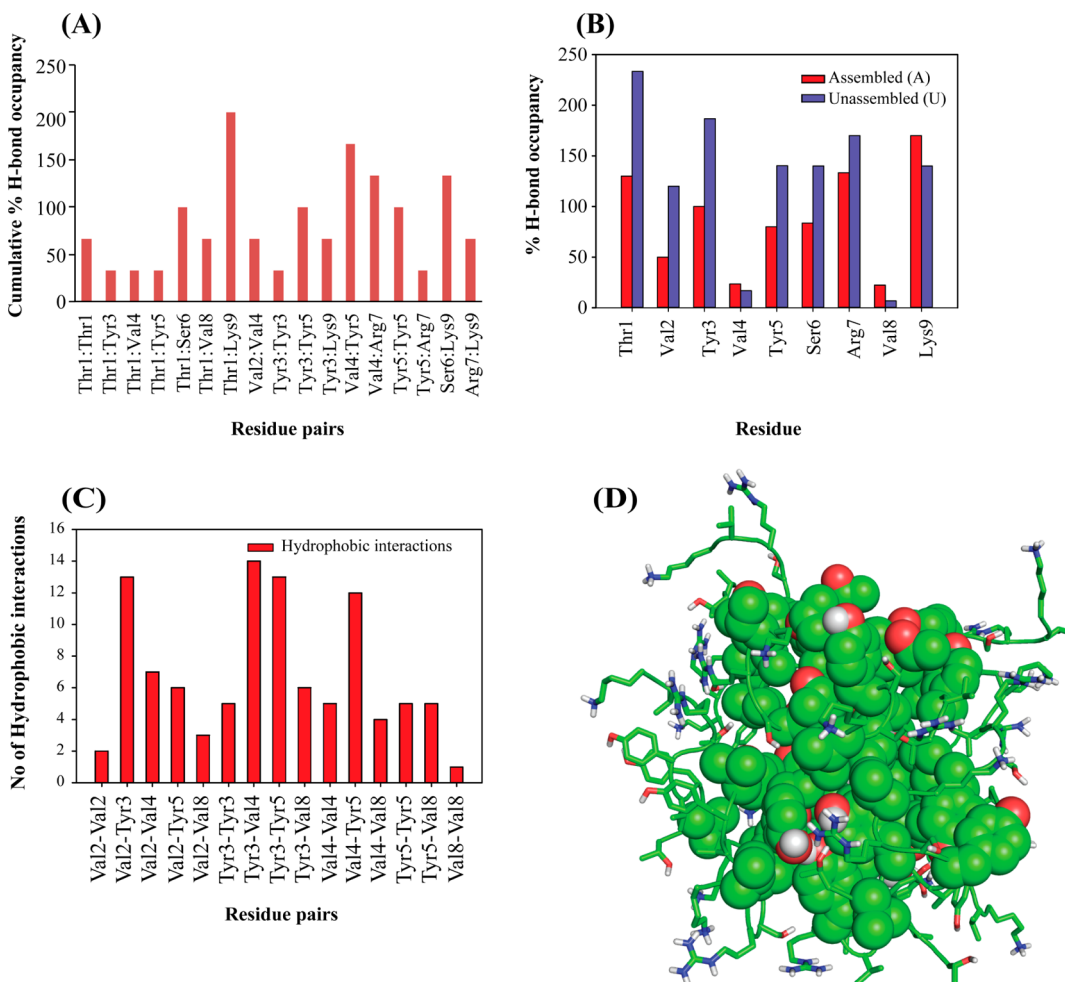


Figure 6. (A) Pairwise hydrogen bond analysis between any two monomers. Cumulative % H bond occupancy is calculated for respective residue pair in each peptide. (B) Percentage of H-bond occupancy of respective residue in each monomer was calculated to understand the amino acid–solvent interactions. Red bar represents the assembled and blue bar represents unassembled aggregation of each monomer of TK9. (C) Total number of hydrophobic interactions for respective residue pair is calculated for all the peptides forming cluster. (D) Oligomeric structure of TK9 is stabilized by hydrophobic hub consisting Tyr, Val, Ser, and Thr residues. Positively charged residues are exposed to water.

The formation of high molecular weight oligomers, associated with an increase in correlation times, (τ_c) is revealed by a decrease in longitudinal relaxation rates (R_1) as reported in Figure 5A for the N-terminal residues of TK9, Val2-Arg7 (Figure 5A). On the other hand, the increase in the aggregation size of the species resulted in an increase in the transverse relaxation rates (R_2) for all the residues of TK9 in the aged sample as compared to that in the freshly prepared sample as

shown in Figure 5B. However, the charged C-terminal residues, Arg7-Val8-Lys9, that are more mobile showed less increment of R_2 values for the aged sample of TK9. Overall, the observed relaxation data suggest the formation of high molecular weight oligomers in aged samples of TK9.

Simulations Suggest That Both Local and Global Orientation of TK9 May Influence Aggregation. The above experimental result motivated us to determine the

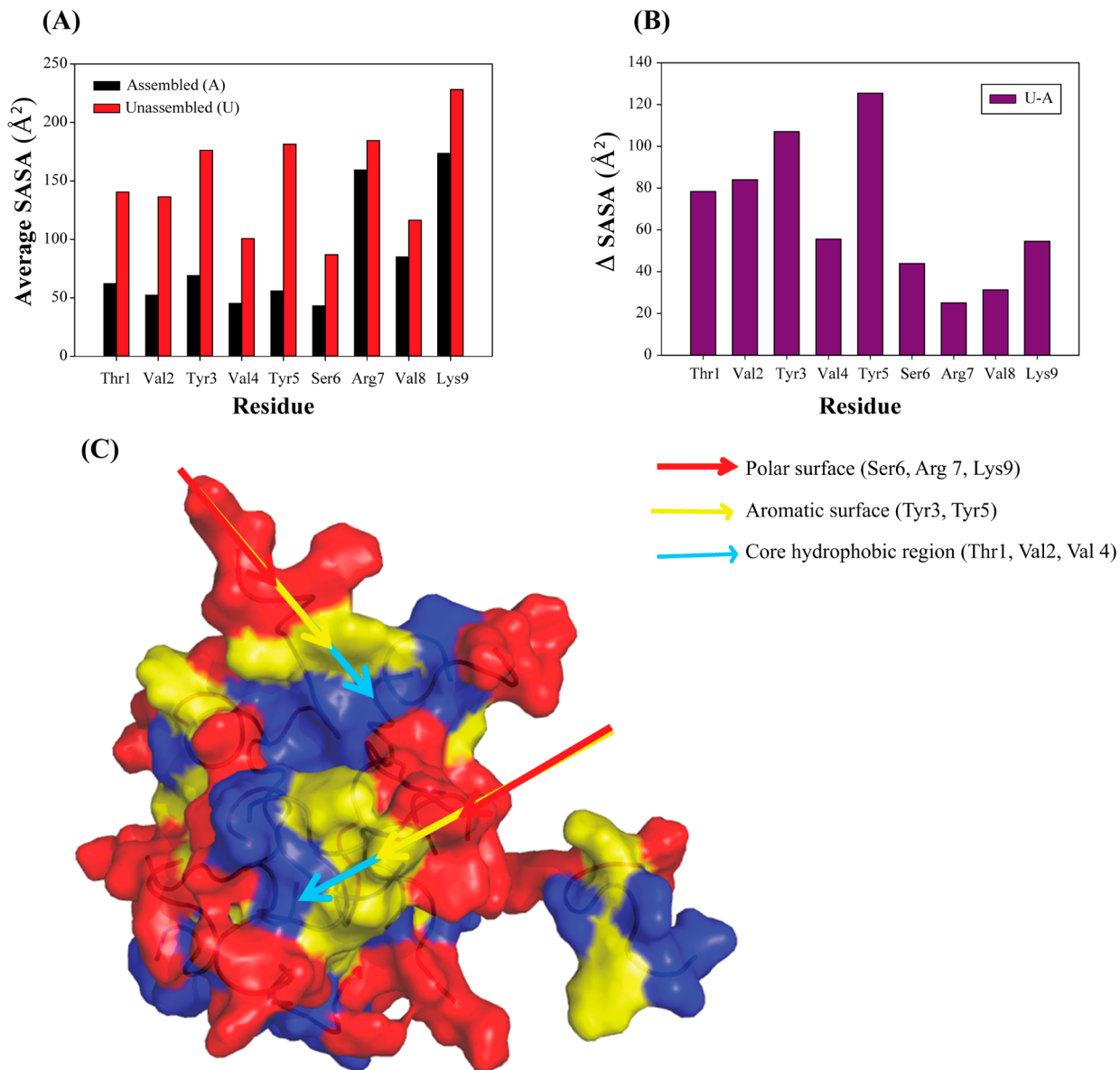


Figure 7. (A) Comparative analysis of the average SASA for each residue in assembled and unassembled state. Black represents the assembled state while red represents the unassembled state. (B) ΔSASA ($\Delta \text{SASA} = \text{SASA}_{\text{unassembled}} - \text{SASA}_{\text{assembled}}$) values for each residue. (C) Surface view of cluster illustrating polarities of residues with color discrimination.

mechanism of aggregation of a small peptide, TK9. Interestingly, among the nine amino acid residues, there are two aromatic amino acid residues, Tyr, three hydrophobic Val residues, two positive charge Lys and Arg, and two β -branched amino acid residues, Thr and Ser. The NMR derived extended conformation of TK9 (Figure S6C) was used as an initial structure for the coarse grained (CG) molecular dynamics (MD) simulation. It is noteworthy to mention that the self-assembly of a short peptide occurs at a microsecond time scale, and hence it is a time-consuming process to carry out all atom MD simulation.⁴⁶ To overcome this problem, coarse-grained MD simulation was adopted to study the aggregation of TK9 with 20 TK9 peptide chains.

Figure S2 summarizes the stages of aggregation of TK9. Interestingly, the scattered monomers started self-assembling after 27 ns of simulation, and the cluster size increased as the time progressed. Finally, after 999 ns of simulation, 15 out of 20 TK9 peptide chains were self-assembled to form the TK9

aggregate (Figure S2). The remaining five TK9 monomers were still scattered after 1 μ s of simulation. Next, we wanted to understand the driving force of the aggregation for TK9. The secondary structure analysis of the assembled as well as the scattered molecules was performed using the Stride web interface.⁴⁷ Interestingly, we found that the 60% of conformation of the assembled peptide possesses a beta turn and more than 35% of conformation exists as random coil (Table S3).

Closer inspection indicated that the self-assembly of TK9 (Figure 6) was stabilized by a variety of interactions, such as H-bonding, electrostatic, π -cation, and van der Waals. The C-terminal positively charged Lys9 residue of TK9 contributed for a H-bonding interaction with Thr1 and with Ser6. In addition, H-bonding contributions were also observed between Thr1-Ser6, Tyr3-Tyr5, Val4-Tyr5, Val2-Val4, and Thr1-Thr1 of TK9 in an assembled state. Apart from the H-bonding interactions between two self-assembled monomers, polar residues such as

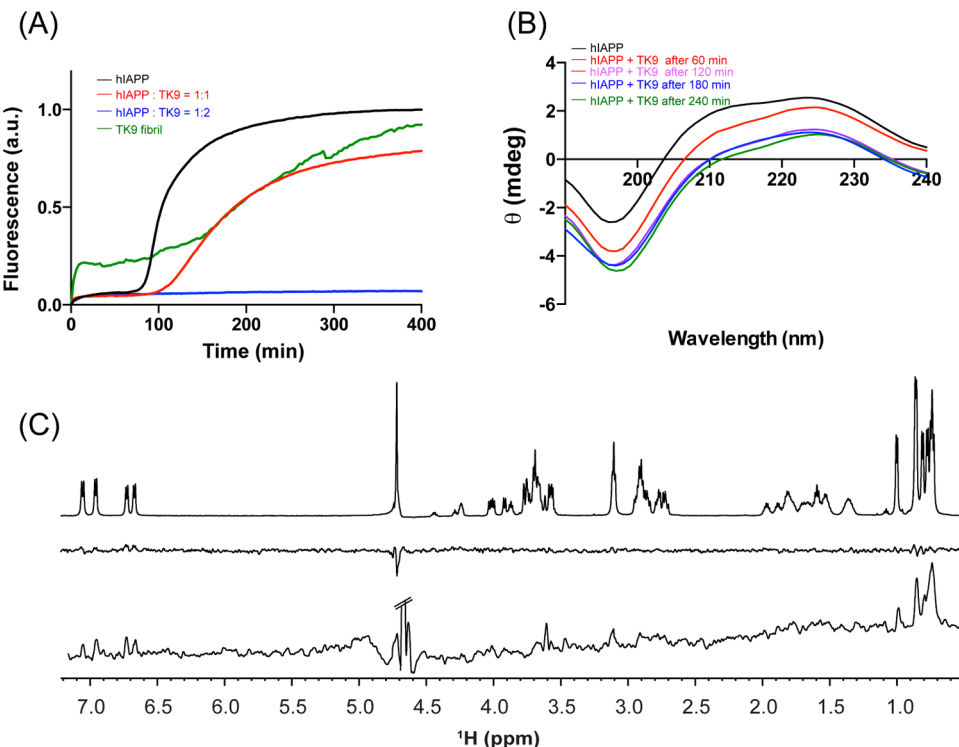


Figure 8. (A) ThT fluorescence assay of hIAPP (black) solution incubated with 1 (red) and 2 (blue) equivalents of TK9; ThT aggregation of TK9 peptide in solution is shown in the green trace. (B) CD spectra of freshly dissolved hIAPP (black) and hIAPP incubated over 6 h with 2 equiv of TK9 at the indicated time intervals of aggregation. (C) One dimensional ^1H NMR spectrum of freshly dissolved TK9 in hIAPP (monomer) (top, control); STD spectrum in the presence of hIAPP monomer at $t = 12$ h (middle) and in the presence of hIAPP fibril (bottom).

614 Arg7 and Lys9 formed numerous intermolecular salt bridge
615 interactions (Table S4). Hydrophobic contacts were also
616 observed between Val2-Tyr3, Val4-Tyr3, Tyr5-Val4, Val2-
617 Val4, Val2-Tyr5, and Tyr3-Val8, which may also play an
618 important role in the aggregated form of TK9 (Figure 6).
619 Interestingly, Tyr3-Tyr3, Tyr5-Tyr5, and Tyr3-Tyr5 aromatic
620 interactions between two monomers of TK9 aggregates were
621 crucial for stabilization. This result was in very good agreement
622 with the Tyr fluorescence intensity enhancement in the
623 aggregated state (Figure 6). A few cation- π interactions
624 between Tyr3-Arg7, Tyr5-Arg7, and Tyr5-Arg9 were also
625 observed in the fibrillar TK9 (Table S5).

626 Solvent accessible surface area (SASA) data were evaluated
627 to suggest the conformation of the biomolecule. The SASA
628 values of each residue of TK9 aggregate as well as in the
629 scattered monomers after 1 μs of simulation were calculated
630 (Figure 7), and it was clear that the overall SASA values for all
631 the residues in the cluster or aggregated form was lower,
632 whereas the same amino acid residues in the scattered peptides
633 (monomer) were much higher. The standard deviation of
634 SASA values of each residue of scattered peptides was less
635 compared to that of aggregated peptides. This behavior could
636 be due to folded conformation in the aggregated form and
637 hence they were less accessible to the solvent. On the other
638 hand, the short peptide TK9 is highly dynamic in nature, and
639 therefore the peptide is more solvent exposed in the unfolded
640 form. Interestingly, the C-terminal residues, Arg7, Val8, and
641 Lys9 showed comparably higher SASA values both in the
642 scattered as well as in the aggregated form (Figure 7). Taken
643 together, the central stabilization of the assembly of TK9 was
644 due to the strong van der Waals interactions between aromatic Tyr
645 hydrophobic Val residues as well as between aromatic Tyr

residues. In comparison, the Arg7 and Lys9 residues of TK9
646 aggregates pointed toward the solvent to form H-bond with the
647 solvent water molecules.
648

TK9 Inhibits hIAPP Aggregation. In order to uncover the
649 potential role of the self-assembling TK9 peptide on amyloid
650 aggregation, it was coincubated with freshly dissolved hIAPP
651 and assayed using ThT to monitor β -sheet rich fibril formation.
652 At a stoichiometric concentration of TK9 monomer, hIAPP still
653 adopted a normal course of aggregation; however, the lag phase
654 was increased and the total fibrillar hIAPP fluorescence
655 intensity was decreased (Figure 8A). With the increased
656 concentration of TK9, hIAPP aggregation was completely
657 diminished. Similarly, incubation of freshly dissolved hIAPP
658 with excess TK9 over 8 h displayed mainly a random coil
659 peptide in solution as shown by CD experiments (Figure 8B).
660 When TK9 fibril was added to hIAPP solution, aggregation of
661 hIAPP was slightly modified, suggesting possible interactions
662 between TK9 and hIAPP.
663

The inhibition of hIAPP aggregation by TK9 was further
664 confirmed by ^1H STD NMR experiments. STD has become a
665 valuable technique to map the interaction of ligands with
666 biomolecules.^{48–50} Freshly prepared hIAPP monomers were
667 added to a solution of TK9 monomers and monitored by NMR
668 for more than 12 h. Receptor, hIAPP, as well as the ligand,
669 TK9, are low-molecular weight molecules; therefore, no STD
670 signals from TK9 in the presence of hIAPP monomers were
671 observed due to the fast tumbling of TK9. However, if hIAPP
672 fibrillizes, it should be possible to transfer the magnetization
673 from the large-size hIAPP fibrils to TK9 peptide in STD
674 experiments. However, the fact that we did not observe the
675 STD signal within a period of 12 h indicates that hIAPP did not
676 exist in fibrillar form (Figure 8C), as hIAPP (in the absence of
677

678 TK9) completely fibrilizes within 3 h at the same condition as
679 seen by the ThT assay (Figure 8C). In addition, when TK9
680 monomers were incubated with hIAPP fibrils, a pronounced
681 STD signal was observed from aromatic as well as aliphatic
682 amino acid residues, indicating that the aromatic and methyl
683 protons are responsible for interacting with fibrillar hIAPP.
684 These observations confirm the ability of TK9 to inhibit hIAPP
685 aggregation to form an ordered secondary structure.

686 ■ DISCUSSION

687 According to the current trend in nanoscience, synthetic
688 amphiphilic small peptides emerge as versatile building block
689 for the fabrication of supramolecular architecture.⁵¹ The ability
690 of these peptides to assemble into ordered nanostructures may
691 help to better understand the natural misfolding pathway of
692 systems such as amyloid proteins.⁵² In these systems, short
693 peptide fragments in the wild-type sequence (KLVFF for
694 amyloid- β and NFGAIL for hIAPP) have been identified to be
695 responsible for β -sheet formation thus more clearly investigat-
696 ing the properties and features of small peptide assemblies can
697 help in better understanding larger protein systems.^{53–55} The
698 self-assembly regions have also served as a template to
699 rationally design amyloid inhibitors by blocking β -sheet
700 formation; therefore, short peptide fragments of amyloid
701 proteins can also help elucidate possible sequence motifs for
702 therapeutic design and development.^{56–58}

703 The aim of this study has been to reveal self-assembly activity
704 of the ultrasmall peptide, TK9 and its variants through
705 biophysical, NMR and computational methods. TK9 and TY5
706 both contain branched, bulky amino acids and a specific
707 sequence (VxVx, Scheme 1) that has been shown to be prone
708 to amyloid-like aggregation.⁵⁹ Over time, TK9 spontaneously
709 aggregated in aqueous solution as seen by DLS (Figure 1) to
710 adopt rod-like fibrillar morphology, confirmed by microscopic
711 studies (Figure 2). Interestingly, the aggregation was β -sheet
712 rich, examined by the increase in ThT fluorescence (Figure 3).
713 All four peptides adopt a random coil monomeric conformation
714 at early time points; however, CD experiments confirmed that
715 TK9 and TY5 form into a β -sheet containing fibrillar species
716 after incubation over days (Figure 1B,C). In addition, because
717 of the presence of the “amyloid aggregation-prone” sequence
718 motif, a further explanation for the aggregation propensity of
719 TK9 and TY5 may be the increase in hydrophobic and aromatic
720 residues, which may favor hydrophobic contacts and $\pi-\pi$
721 interactions as well as undergo a transition to β -sheet during
722 self-assembly more readily than peptides with aliphatic
723 residues.⁵⁹

724 Structurally different, YRS and SK4, which do not contain
725 the aggregation-prone sequence, did not show this transition to
726 β -sheet, nor did they show an enhanced ThT fluorescence,
727 suggesting an ill-defined secondary structure. The distribution
728 profile of the peptides is also varied upon aggregation as
729 suggested by the DLS studies (Figure 1A). As the peptides
730 were incubated, the size of the species increased, which may be
731 attributed to the fibril-like aggregates formed in the case of TK9
732 and TY5. The $\pi-\pi$ interactions could be the governing factor
733 for the folding of the peptide into supramolecular assemblies as
734 seen by Tyr fluorescence experiments (Figure 3). As TK9 is
735 allowed to self-assemble, it forms a hydrophobic core, which
736 does not allow for interactions with water, and thus an
737 enhancement in the Tyr fluorescence signal by neighboring Tyr
738 residues. Coarse grain MD simulation confirms that the self-
739 assembled oligomer of TK9 is stabilized by hydrophobic amino

740 acid residues such as Tyr and Val from individual monomers to
741 form a hydrophobic hub and all the charge residues such as
742 Arg7 and Lys9 are exposed to water (Figure 6). In contrary, the
743 solvent quenches the fluorescence intensity of TK9 or TY5
744 monomer (Figure 3). However, a well-defined secondary
745 structure of YRS, the central region of TK9, was not observed.
746 In order to probe the mechanistic insights of self-assembly of a
747 short peptide at an atomic resolution, NMR spectroscopy was
748 carried out.

749 Proton NMR and relaxation studies further confirm the
750 presence of high molecular weight oligomers in aged samples.
751 In ^1H NMR spectra, amide resonances are observed for all of
752 the peptides at initial time points. As the peptides are allowed
753 to self-assemble, significant line broadening is visible for TK9
754 and TY5, whereas a lesser broadening is seen for YRS and SK4
755 over the time course (Figure 4). The line broadening observed
756 for TK9 or TY5 peptides confirms the low correlation times
757 with millisecond to microsecond time scale of motion between
758 several states of micelle-like aggregation. This dynamic behavior
759 may further confirm an aggregation process occurring in
760 solution, specifically the formation of high molecular weight
761 assemblies that tumble slowly in NMR time scale, which gave
762 rise to an increased rotational correlation time (Figure 5). The
763 TOCSY and ROSEY data, taken of freshly prepared monomers,
764 show no medium or long-range cross peaks (or ROEs),
765 confirming the absence of a well-defined secondary structure
766 (possibly random coil) prior to incubation (Figure S6).

767 Furthermore, the applications of these self-assembled
768 peptides are of great value since they do have interesting
769 intrinsic properties; however, their role in understanding
770 protein–protein interactions may also be useful. Investigations
771 of the interaction between amyloid proteins and other
772 biologically relevant proteins have been of great interest.
773 Specifically, reports regarding the interaction of cosecreted
774 proteins, hIAPP and insulin, has shed light into the involvement
775 of a protein on amyloid formation.^{60,61} Aforementioned, small
776 peptide sequence from the native protein have been utilized in
777 the design of amyloid inhibitors due to their ability to contain
778 self-recognition motifs which can interact with the target
779 protein through hydrophobic and electrostatic interactions and
780 prevent polymerization to fibrils.^{56,62,63} In order to study this,
781 we tested the inhibitory activity of TK9 against hIAPP, an
782 amyloid protein suggested to be a pathological feature of type-2
783 diabetes. Our experimental results indicate that the amyloid-
784 inhibition properties of TK9 monomers are concentration
785 dependent as shown in Figure 8. This observation is similar to
786 that shown for amyloid-inhibiting properties of a nine-residue
787 peptide, NK9 (or $^{45}\text{NIVNVSLVK}^{53}$) adopted from SARS CoV
788 E-protein, against the fibrillation of insulin.⁶⁴ Interestingly, TK9
789 monomers are able to modify the aggregation kinetics of hIAPP
790 and completely inhibit the fibril formation upon incubation
791 with an excess amount of a TK9. This result was further verified
792 by STD NMR experiments, which showed that upon
793 incubation of hIAPP monomers with excess TK9 monomers,
794 no pronounced STD effect was observed indicating the
795 presence of a small, insufficient amount of hIAPP fibers. On
796 the other hand, when TK9 monomers are present in a solution
797 along with hIAPP fibrils, a strong STD signal was observed,
798 confirming an interaction between the two peptides.

799 Overall, the study of self-assembled peptides nanostructures
800 can serve, as useful systems for understanding more global
801 systems, like amyloid proteins kinetics and aggregation at the
802 atomic level. Herein, the aggregation properties of TK9 and its

variants were characterized through biophysical, spectroscopic, and simulated studies, and it was confirmed that the structure of these peptides influence their aggregation propensity and fibrillar morphology. TK9 underwent a transition to a more β -sheet-rich structure, which adopted a fibril-like shape. These aggregates were further investigated through simulations to understand more clearly the possible intra- and interpeptide interactions at the molecular level. As described here, self-assembly peptides may also be useful templates for designing amyloid inhibitor. These self-assembly systems may also be used in understanding the molecular and structural biology, which will inspire the design and synthesis of increasingly complex self-assembled biomaterials for biomedicine. Furthermore, investigations to probe the structural characteristics of these peptides in the presence of membrane can also be of great value since the amyloid beta or hIAPP protein interacts with membrane before going to fibrillation.^{65–67} Therefore, instead of using the entire protein of amyloid- β or hIAPP in membrane, this peptide can be a nanoindicator to understand the structural insight at the membrane surface for the mechanism of the fibrillation process.

ASSOCIATED CONTENT

Supporting Information

Simulation parameters, structural statistics and models, NMR structure and figures referenced in the text. This material is available free of charge via the Internet at <http://pubs.acs.org>.

AUTHOR INFORMATION

Corresponding Author

*E-mail: bhunia@jcbose.ac.in; abhunia@umich.edu.

Author Contributions

[§]Both authors (A.G. and A.S.P.) contributed equally.

Funding

A.B. would like to thank Bose Institute, Kolkata, India, for financial support. A.G. thanks CSIR, Govt. of India for senior research fellowship. S.B. thanks Bose Institute, Kolkata for an M.Sc.–Ph.D fellowship. Central instrument facility (CIF) of Bose Institute is greatly acknowledged. Part of this study, and A.B. and A.S.P. were supported by funds from NIH (GM084018 to A.R.).

Notes

The authors declare no competing financial interest.

ABBREVIATIONS

hIAPP, human islet amyloid polypeptide protein; DLS, dynamic light scattering; CD, circular dichroism; NMR, nuclear magnetic resonance; MD, molecular dynamics simulation; SEM, scanning electron microscopy; ROESY, rotating frame nuclear Overhauser effect spectroscopy; STD, saturation transfer difference spectroscopy; TEM, transmission electron microscopy; ThT, thioflavin T; TOCSY, total correlation spectroscopy

REFERENCES

- (1) Gazit, E. (2007) Self-assembled peptide nanostructures: the design of molecular building blocks and their technological utilization. *Chem. Soc. Rev.* 36, 1263–1269.
- (2) Zhao, X., Pan, F., Xu, H., Yaseen, M., Shan, H., Hauser, C. A., Zhang, S., and Lu, J. R. (2010) Molecular self-assembly and applications of designer peptide amphiphiles. *Chem. Soc. Rev.* 39, 3480–3498.
- (3) Zhang, S. (2003) Fabrication of novel biomaterials through molecular self-assembly. *Nat. Biotechnol.* 21, 1171–1178.
- (4) Whitesides, G., Mathias, J., and Seto, C. (1991) Molecular self-assembly and nanochemistry: a chemical strategy for the synthesis of nanostructures. *Science* 254, 1312–1319.
- (5) Lecommandoux, S., Achard, M.-F., Langenwalter, J. F., and Klok, H.-A. (2001) Self-assembly of rod-coil diblock oligomers based on α -helical peptides. *Macromolecules* 34, 9100–9111.
- (6) Lawrence, D. S., Jiang, T., and Levett, M. (1995) Self-assembling supramolecular complexes. *Chem. Rev.* 95, 2229–2260.
- (7) Bhunia, A., Saravanan, R., Mohanram, H., Mangoni, M. L., and Bhattacharjya, S. (2011) NMR structures and interactions of temporin-1TI and temporin-1Tb with lipopolysaccharide micelles: mechanistic insights into outer membrane permeabilization and synergistic activity. *J. Biol. Chem.* 286, 24394–24406.
- (8) Saravanan, R., Joshi, M., Mohanram, H., Bhunia, A., Mangoni, M. L., and Bhattacharjya, S. (2013) NMR structure of temporin 1 Ta in lipopolysaccharide micelles: mechanistic insights into inactivation by outer membrane. *PLoS One* 8, e72718.
- (9) Lakshmanan, A., Zhang, S., and Hauser, C. A. (2012) Short self-assembling peptides as building blocks for modern nanodevices. *Trends Biotechnol.* 30, 155–165.
- (10) Hosseinkhani, H., Hong, P.-D., and Yu, D.-S. (2013) Self-assembled proteins and peptides for regenerative medicine. *Chem. Rev.* 113, 4837–4861.
- (11) Yemini, M., Reches, M., Rishpon, J., and Gazit, E. (2005) Novel electrochemical biosensing platform using self-assembled peptide nanotubes. *Nano Lett.* 5, 183–186.
- (12) Ross, C. A., and Poirier, M. A. (2004) *Nat. Med.* 10, S10–S17.
- (13) Knowles, T. P., Vendruscolo, M., and Dobson, C. M. (2014) The amyloid state and its association with protein misfolding diseases. *Nat. Rev. Mol. Cell Biol.* 15, 384–396.
- (14) Chiti, F., and Dobson, C. M. (2006) Protein misfolding, functional amyloid, and human disease. *Annu. Rev. Biochem.* 75, 333–366.
- (15) Lu, K., Jacob, J., Thiagarajan, P., Conticello, V. P., and Lynn, D. G. (2003) Exploiting amyloid fibril lamination for nanotube self-assembly. *J. Am. Chem. Soc.* 125, 6391–6393.
- (16) Wilson, L., McKinlay, C., Gage, P., and Ewart, G. (2004) SARS coronavirus E protein forms cation-selective ion channels. *Virology* 330, 322–331.
- (17) Verdiá-Baguena, C., Nieto-Torres, J. L., Alcaraz, A., DeDiego, M. L., Torres, J., Aguilera, V. M., and Enjuanes, L. (2012) Coronavirus E protein forms ion channels with functionally and structurally involved membrane lipids. *Virology* 432, 485–494.
- (18) Li, Y., Surya, W., Claudine, S., and Torres, J. (2014) Structure of a Conserved Golgi Complex-targeting Signal in Coronavirus Envelope Proteins. *J. Biol. Chem.* 289, 12535–12549.
- (19) Chan, W. C., and White, P. D. (2000) *Fmoc Solid Phase Peptide Synthesis*; Oxford University Press, New York.
- (20) Ghosh, A., Datta, A., Jana, J., Kar, R. K., Chatterjee, C., Chatterjee, S., and Bhunia, A. (2014) Sequence context induced antimicrobial activity: insight into lipopolysaccharide permeabilization. *Mol. BioSyst.* 10, 1596–1612.
- (21) Lakowicz, J. R. (2007) *Principles of Fluorescence Spectroscopy*, Springer, Berlin.
- (22) Goddard, T., and Kneller, D. (2004) SPARKY 3, University of California: San Francisco, 14, 15.
- (23) Güntert, P. (2004) Automated NMR structure calculation with CYANA, In *Protein NMR Techniques*, pp 353–378, Springer, Berlin.
- (24) Ghosh, A., Kar, R. K., Jana, J., Saha, A., Jana, B., Krishnamoorthy, J., Kumar, D., Ghosh, S., Chatterjee, S., and Bhunia, A. (2014) Indolicidin Targets Duplex DNA: Structural and Mechanistic Insight through a Combination of Spectroscopy and Microscopy. *ChemMedChem* 9, 2052–2058.
- (25) Ghosh, A., Kar, R. K., Krishnamoorthy, J., Chatterjee, S., and Bhunia, A. (2014) Double GC: GC Mismatch in dsDNA Enhances Local Dynamics Retaining the DNA Footprint: A High-Resolution NMR Study. *ChemMedChem* 9, 2059–2064.

- 930 (26) Marrink, S. J., de Vries, A. H., and Mark, A. E. (2004) Coarse
931 grained model for semiquantitative lipid simulations. *J. Phys. Chem. B*
932 108, 750–760.
- 933 (27) Marrink, S. J., Risselada, H. J., Yefimov, S., Tieleman, D. P., and
934 de Vries, A. H. (2007) The MARTINI force field: coarse grained
935 model for biomolecular simulations. *J. Phys. Chem. B* 111, 7812–7824.
- 936 (28) Hess, B., Kutzner, C., Van Der Spoel, D., and Lindahl, E. (2008)
937 GROMACS 4: Algorithms for highly efficient, load-balanced, and
938 scalable molecular simulation. *J. Chem. Theory Comput.* 4, 435–447.
- 939 (29) Rzepiela, A. J., Schäfer, L. V., Goga, N., Risselada, H. J., De
940 Vries, A. H., and Marrink, S. J. (2010) Reconstruction of atomistic
941 details from coarse-grained structures. *J. Comput. Chem.* 31, 1333–
942 1343.
- 943 (30) Hoover, W. G. (1985) Canonical dynamics: equilibrium phase-
944 space distributions. *Phys. Rev. A* 31, 1695.
- 945 (31) Oostenbrink, C., Villa, A., Mark, A. E., and Van Gunsteren, W.
946 F. (2004) A biomolecular force field based on the free enthalpy of
947 hydration and solvation: The GROMOS force-field parameter sets
948 53A5 and 53A6. *J. Comput. Chem.* 25, 1656–1676.
- 949 (32) Cohen, J. R., Lin, L. D., and Machamer, C. E. (2011)
950 Identification of a Golgi complex-targeting signal in the cytoplasmic
951 tail of the severe acute respiratory syndrome coronavirus envelope
952 protein. *J. Virol.* 85, 5794–5803.
- 953 (33) Fukushi, S., Mizutani, T., Sakai, K., Saijo, M., Taguchi, F.,
954 Yokoyama, M., Kurane, I., and Morikawa, S. (2007) Amino acid
955 substitutions in the s2 region enhance severe acute respiratory
956 syndrome coronavirus infectivity in rat angiotensin-converting enzyme
957 2-expressing cells. *J. Virol.* 81, 10831–10834.
- 958 (34) Nieto-Torres, J. L., DeDiego, M. L., Álvarez, E., Jiménez-
959 Guardeño, J. M., Regla-Nava, J. A., Llorente, M., Kremer, L., Shuo, S.,
960 and Enjuanes, L. (2011) Subcellular location and topology of severe
961 acute respiratory syndrome coronavirus envelope protein. *Virology*
962 415, 69–82.
- 963 (35) Ruch, T. R., and Machamer, C. E. (2011) The hydrophobic
964 domain of infectious bronchitis virus E protein alters the host secretory
965 pathway and is important for release of infectious virus. *J. Virol.* 85,
966 675–685.
- 967 (36) Halverson, K., Fraser, P. E., Kirschner, D. A., and Lansbury, P.
968 T., Jr. (1990) Molecular determinants of amyloid deposition in
969 Alzheimer's disease: conformational studies of synthetic beta-protein
970 fragments. *Biochemistry* 29, 2639–2644.
- 971 (37) Remington, J. S., Klein, J. O., Wilson, C. B., Nizet, V., and
972 Maldonado, Y. (2001) Infectious diseases of the fetus and newborn.
973 *Infect. Dis. Fetus Newborn* 12, 643–681.
- 974 (38) Do, T. D., LaPointe, N. E., Sangwan, S., Teplow, D. B.,
975 Feinstein, S. C., Sawaya, M. R., Eisenberg, D. S., and Bowers, M. T.
976 (2014) Factors that drive peptide assembly from native amyloid
977 structures: experimental and theoretical analysis of [leu-5]-enkephalin
978 mutants. *J. Phys. Chem. B* 118, 7247–7256.
- 979 (39) Ye, W., Chen, Y., Wang, W., Yu, Q., Li, Y., Zhang, J., and Chen,
980 H. F. (2012) Insight into stability of cross-beta amyloid fibril from
981 VEALYL short peptide with molecular dynamics simulations. *PLoS*
982 *One* 7, e36382.
- 983 (40) Do, T. D., LaPointe, N. E., Economou, N. J., Buratto, S. K.,
984 Feinstein, S. C., Shea, J. E., and Bowers, M. T. (2013) Effects of pH
985 and charge state on peptide assembly: the YVIFL model system. *J.*
986 *Phys. Chem. B* 117, 10759–10768.
- 987 (41) Zheng, J., Baghkhalian, A. M., and Nowick, J. S. (2013) A
988 hydrophobic surface is essential to inhibit the aggregation of a tau-
989 protein-derived hexapeptide. *J. Am. Chem. Soc.* 135, 6846–6852.
- 990 (42) Berne, B. J., and Pecora, R. (2000) *Dynamic Light Scattering:
991 with Applications to Chemistry, Biology, and Physics*; Courier Dover
992 Publications, Mineola, NY.
- 993 (43) Westermark, P., Engström, U., Johnson, K. H., Westermark, G.
994 T., and Betsholtz, C. (1990) Islet amyloid polypeptide: pinpointing
995 amino acid residues linked to amyloid fibril formation. *Proc. Natl. Acad.*
996 *Sci. U.S.A.* 87, 5036–5040.
- 997 (44) Levine, H. (1993) Thioflavine T interaction with synthetic
998 Alzheimer's disease beta-amyloid peptides: Detection of amyloid
999 aggregation in solution. *Protein Sci.* 2, 404–410.
- 999 (45) Esposito, V., Das, R., and Melacini, G. (2005) Mapping
1000 polypeptide self-recognition through 1H off-resonance relaxation. *J. Am. Chem. Soc.* 127, 9358–9359.
- 1000 (46) Klein, M. L., and Shinoda, W. (2008) Large-scale molecular
1003 dynamics simulations of self-assembling systems. *Science* 321, 798–
1004 800.
- 1006 (47) Heinig, M., and Frishman, D. (2004) STRIDE: a web server for
1007 secondary structure assignment from known atomic coordinates of
1008 proteins. *Nucleic Acids Res.* 32, W500–W502.
- 1009 (48) Bhunia, A., Bhattacharjya, S., and Chatterjee, S. (2012) Applications
1010 of saturation transfer difference NMR in biological systems. *Drug Discovery Today* 17, 505–513.
- 1012 (49) Mayer, M., and Meyer, B. (1999) Characterization of ligand
1013 binding by saturation transfer difference NMR spectroscopy. *Angew. Chem., Int. Ed.* 38, 1784–1788.
- 1015 (50) Yesuvadian, R., Krishnamoorthy, J., Ramamoorthy, A., and
1016 Bhunia, A. (2014) Potent gamma-secretase inhibitors/modulators interact
1017 with amyloid-beta fibrils but do not inhibit fibrillation: A high-resolution
1018 NMR study. *Biochem. Biophys. Res. Commun.* 447, 590–595.
- 1019 (51) Rajagopal, K., and Schneider, J. P. (2004) Self-assembling
1020 peptides and proteins for nanotechnological applications. *Curr. Opin. Struct. Biol.* 14, 480–486.
- 1022 (52) Dobson, C. M. (2003) Protein folding and misfolding. *Nature*
1023 426, 884–890.
- 1024 (53) Tjernberg, L. O., Näslund, J., Lindqvist, F., Johansson, J.,
1025 Karlström, A. R., Thyberg, J., Terenius, L., and Nordstedt, C. (1996)
1026 Arrest of amyloid fibril formation by a pentapeptide ligand. *J. Biol. Chem.* 271, 8545–8548.
- 1028 (54) Kapurniotu, A., Schmauder, A., and Tenidis, K. (2002)
1029 Structure-based design and study of non-amyloidogenic, double N-
1030 methylated IAPP amyloid core sequences as inhibitors of IAPP
1031 amyloid formation and cytotoxicity. *J. Mol. Biol.* 315, 339–350.
- 1032 (55) Gazit, E. (2007) Self assembly of short aromatic peptides into
1033 amyloid fibrils and related nanostructures. *Prion* 1, 32–35.
- 1034 (56) Tatarek-Nossol, M., Yan, L.-M., Schmauder, A., Tenidis, K.,
1035 Westermark, G., and Kapurniotu, A. (2005) Inhibition of hIAPP
1036 amyloid-fibril formation and apoptotic cell death by a designed hIAPP
1037 amyloid-core-containing hexapeptide. *Chem. Biol.* 12, 797–809.
- 1038 (57) Watanabe, K.-i., Nakamura, K., Akikusa, S., Okada, T., Kodaka,
1039 M., Konakahara, T., and Okuno, H. (2002) Inhibitors of fibril
1040 formation and cytotoxicity of beta-amyloid peptide composed of KLVFF
1041 recognition element and flexible hydrophilic disrupting element. *Biochem. Biophys. Res. Commun.* 290, 121–124.
- 1042 (58) Gazit, E. (2005) Mechanisms of amyloid fibril self-assembly and
1043 inhibition. *FEBS J.* 272, 5971–5978.
- 1044 (59) de la Paz, M. L., and Serrano, L. (2004) Sequence determinants
1045 of amyloid fibril formation. *Proc. Natl. Acad. Sci. U.S.A.* 101, 87–92.
- 1046 (60) Brender, J. R., Lee, E. L., Hartman, K., Wong, P. T.,
1047 Ramamoorthy, A., Steel, D. G., and Gafni, A. (2011) Biphasic effects
1048 of insulin on islet amyloid polypeptide membrane disruption. *Biophys. J.* 100,
1049 685–692.
- 1051 (61) Susa, A. C., Wu, C., Bernstein, S. L., Dupuis, N. F., Wang, H.,
1052 Raleigh, D. P., Shea, J.-E., and Bowers, M. T. (2014) Defining the
1053 Molecular Basis of Amyloid Inhibitors: Human Islet Amyloid
1054 Polypeptide–Insulin Interactions. *J. Am. Chem. Soc.* 136, 12912–
1055 12919.
- 1056 (62) Tjernberg, L. O., Lilliehöök, C., Callaway, D. J., Näslund, J.,
1057 Hahne, S., Thyberg, J., Terenius, L., and Nordstedt, C. (1997)
1058 Controlling amyloid beta-peptide fibril formation with protease-stable
1059 ligands. *J. Biol. Chem.* 272, 12601–12605.
- 1060 (63) Mishra, A., Misra, A., Vaishnavi, T. S., Thota, C., Gupta, M.,
1061 Ramakumar, S., and Chauhan, V. S. (2013) Conformationally
1062 restricted short peptides inhibit human islet amyloid polypeptide
1063 (hIAPP) fibrilization. *Chem. Commun.* 49, 2688–2690.
- 1064 (64) Banerjee, V., Kar, R. K., Datta, A., Parthasarathi, K., Chatterjee,
1065 S., Das, K. P., and Bhunia, A. (2013) Use of a small peptide fragment
1065

- 1066 as an inhibitor of insulin fibrillation process: A study by high and low
1067 resolution spectroscopy. *PloS One* 8, e72318.
- 1068 (65) Brender, J. R., Salamekh, S., and Ramamoorthy, A. (2011)
1069 Membrane disruption and early events in the aggregation of the
1070 diabetes related peptide IAPP from a molecular perspective. *Acc. Chem.*
1071 *Res.* 45, 454–462.
- 1072 (66) Patel, H. R., Pithadia, A. S., Brender, J. R., Fierke, C. A., and
1073 Ramamoorthy, A. (2014) In Search of Aggregation Pathways of IAPP
1074 and other Amyloidogenic Proteins: Finding Answers Through NMR
1075 Spectroscopy. *J. Phys. Chem. Lett.* 5, 1864–1870.
- 1076 (67) Qiang, W., Akinlolu, R. D., Nam, M., and Shu, N. (2014)
1077 Structural Evolution and Membrane Interaction of the 40-Residue beta
1078 Amyloid Peptides: Differences in the Initial Proximity between
1079 Peptides and the Membrane Bilayer Studied by Solid-State Nuclear
1080 Magnetic Resonance Spectroscopy. *Biochemistry* 53, 7503–7514.